What is the relationship between the wrap angle of a capstan and the loading force?

Abraham Cheung

Introduction

A capstan is a device on a ship which increases the loading force of a rope by wrapping it around a cylinder, allowing sailors to control the movement of a huge load with little loading force. Microscopically, a portion of the holding force is distributed across the surface of the capstan as normal forces, known as the Capstan equation. This effect has led to a wide variety of applications, including windlasses, which are used to raise heavy masses, and provides an understanding of frictional forces in conveyor belts. Understanding the correct wrap angle of a capstan can help determine the minimum loading force, which can help prevent injuries in rock climbing activities or rescue missions.

Although the classical Capstan equation gives a good approximation of the relationship between the hold force and the load force, several assumptions such as the rope being non-elastic and non-rigid is often hard to be fulfilled. In fact, Gao et al. has observed an experimental discrepancy of up to 12.58%, while Ramkumar et al. observed that the normal force of a string is not proportional to its frictional force, with the p-value of 8.29×10^{-8}, below the statistically significant p-value of 0.05. Therefore, assessing the relationship would allow us to better apply the relationship in real-life applications.

Framework

The following section aims to derive the classical Capstan Equation:

$$T_{hold} = T_{load}e^{-\mu_s\theta} \tag{1}$$

Suppose a small sector of the cross-sectional area of the capstan, for a small angle $\Delta\theta$, the angle that the string forms with the tangent of the circle is $\frac{\Delta\theta}{2}$:
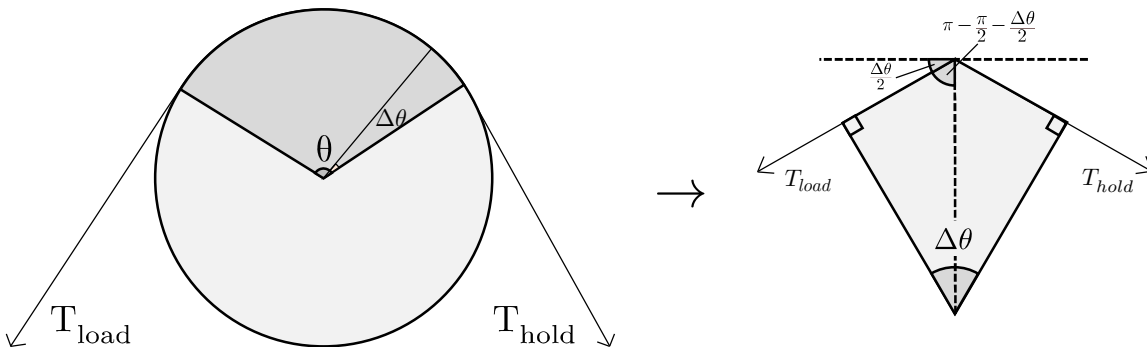
Figure 1. A capstan (left) and its sector depicted as a section of a n-gon as $n \to \infty$ (right).

To find the minimum amount of loading tension (T_{load}) needed for the rope to not slip, the system has to be in equilibrium, in other words, the sum of forces in all directions must be 0.
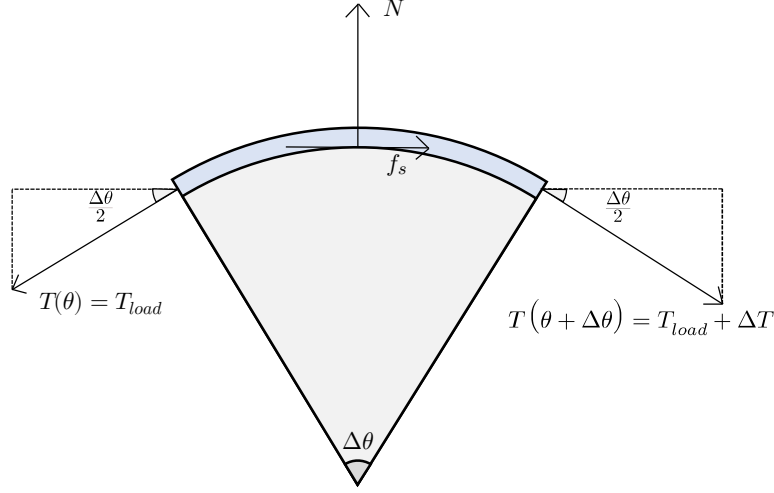
Figure 2. A free-body force diagram depicting the forces acting on a small sector of the capstan.

By decomposing the force vectors, the sum of horizontal forces is 0:

$$F_x = 0$$

$$-T_{load}\cos\left(\frac{\Delta\theta}{2}\right) + f_s + (T_{load} + \Delta T)\cos\left(\frac{\Delta\theta}{2}\right) = 0 \tag{2}$$

Using the small angle approximation of $cos(\frac{\Delta\theta}{2}) \cong 1$, Equation (2) becomes:

$$-T_{load} + f_s + (T_{load} + \Delta T) = 0$$

$$f_s = -\Delta T \tag{3}$$

The sum of vertical forces is also 0:

$$F_y = 0$$

$$-T_{load}\sin\left(\frac{\Delta\theta}{2}\right) + N - (T_{load} + \Delta T)\sin\left(\frac{\Delta\theta}{2}\right) = 0 \tag{4}$$

Using the small angle approximation of $sin(\frac{\Delta\theta}{2}) \cong \frac{\Delta\theta}{2}$, Equation (4) becomes:

$$-T_{load}\left(\frac{\Delta\theta}{2}\right) + N - (T_{load} + \Delta T)\left(\frac{\Delta\theta}{2}\right) = 0$$

$$N = \Delta T\frac{\Delta\theta}{2} + T_{load}\Delta\theta \tag{5}$$

Amonton's Classic Law of Friction states that:

$$f_s = \mu_s N \tag{6}$$

Substituting (3) and (5) and into (6):

$$-\Delta T = \mu_s\left(\Delta T\frac{\Delta\theta}{2} + T_{load}\Delta\theta\right)$$

$$\lim_{(\Delta T,\Delta\theta)\to(0,0)}\frac{\Delta T}{\Delta\theta} = \lim_{(\Delta T,\Delta\theta)\to(0,0)} -\mu_s\left(\frac{\Delta T}{2} + T_{load}\right)$$

$$\frac{dT}{d\theta} = -\mu_s T_{load} \tag{7}$$

Solving the differential equation by integrating both sides, from $\theta = 0$ to $\theta = \theta$, and from $T_{load} = \text{T}_{\text{load}}$ to $T_{load} = \text{T}_{\text{hold}}$, the relationship between the loading force and holding force can be related over the wrap angle θ:

$$\int_{T_{load}=\text{T}_{\text{load}}}^{T_{load}=\text{T}_{\text{hold}}} \frac{dT}{T_{load}} = -\mu_s \int_{\theta=0}^{\theta=\theta} d\theta$$
$$\ln T_{hold} - \ln T_{load} = -\mu_s\theta$$
$$\frac{T_{hold}}{T_{load}} = e^{-\mu_s\theta}$$
$$T_{hold} = T_{load}e^{-\mu_s\theta} \tag{8}$$

There are several assumptions in this relationship:

1. The string obeys Amonton's Classic Law of Friction, as described in (6), where static frictional force (f_s) is proportional to the normal force (N).
2. The string is non-rigid, meaning zero force is needed to bend the string around the capstan, as this affects the normal force (N).
3. The string is non-elastic, as this may affect the coefficient of friction (μ_s).
4. The holding force (T_{hold}) is the absolute minimum tension required for the string to not slip, or be in equilibrium, for a given loading force (T_{load}).

Variables

Type	Name	Symbol	Description
Independent (Raw)	Coordinates of string in image	x_1, y_1 x_2, y_2 x_3, y_3 x_4, y_4	Four sets of coordinates that marks the important ends of the string. The image is first passed through a Sobel Operator[1] and GIMP[2] is then used to manually mark the coordinates.
Independent	Wrap Angle	θ	The subtended angle of a sector of a capstan, where the string is in direct contact with the surface, as shown in Figure 1. This is measured by processing the four sets of coordinates into a series of trigonometric functions, detailed in the Appendix.
Dependent	Holding Force	T_{hold}	The source of tension of the string. This is kept constant by using the same slotted mass and ensuring that it does not move or rotate during each trial.
Controlled	Loading force	T_{load}	The minimum force required to hold the mass without the rope slipping. This is measured by attaching a dual-range force sensor to the end of a string and allowing the holding mass to exert tension onto the string.
Controlled	Static coefficient of friction	μ_s	The proportionality constant that relates the loading force to the holding force. This is kept constant by using the same string and capstan during each trial.
Controlled	Time	t	The time in which the holding force is applied to the string. A stopwatch is used to prevent unnecessary long periods of stress on the string, affecting its elasticity or its static coefficient of friction.

---

[1] A Sobel Operator is an edge-detecting algorithm emphasizes the edges of an image, hence allowing a higher accuracy when manually determining the position of the string, available at https://shd101wyy.github.io/edge-detection/.

[2] An open-source image-processing software, available at https://gimp.org.

Pilot Study

The classical Capstan Equation states that $T_{hol} = T_{load}e^{-\mu_s\theta}$, showing as the wrap angle (θ) increases, the loading force (T_{load}) decreases logarithmically:
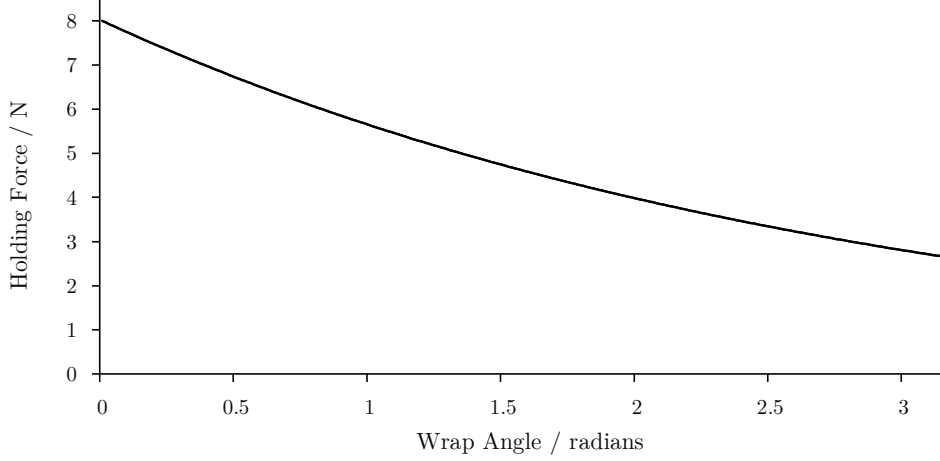
Figure 3. A plot of the Capstan equation, where $T_{load} = 8\ N$ and $\mu_s = 0.35$ (Gao et al.)

As the wrap angle tends towards 0, it approaches the loading force, therefore determining a suitable value of the loading force is important. According to the specifications of the Vernier dual-range force sensor, it has a 0.01N resolution at $\pm$10N range, and a 0.05N resolution at $\pm$50N range. According to a research by Huang et al., the tensile strength of two-ply cotton yarn, or the maximum force at which the string breaks is 27.27N. To minimise the risk of accidents and to minimise the percentage error, it has been decided to keep the loading force at approximately 8N:
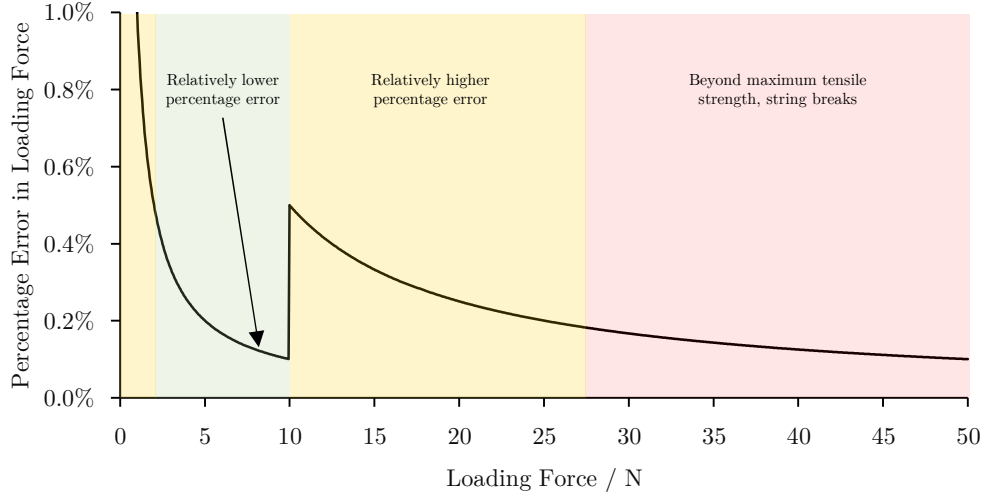
Figure 4. A plot of the percentage error in the measured loading force against the true loading force.

The loading force of 10N exactly is not chosen because the force sensor will be zero-calibrated at the start of each experiment, meaning a potential wrong assumption of the absolute uncertainty.

As for the range of independent variables, it has been decided to perform 7 regular intervals of the wrap angle from $0 \le \theta \le \frac{7\pi}{4}$. With reference to Figure 3, because the magnitude of the change in holding force over the change in wrap angle is relatively low, the significant of studying the holding force beyond $\theta = \frac{7\pi}{4}$ would be minimal.

Apparatus

4x G-clamp	**1x** 2-ply cotton yarn	**1x** 800g slotted mass
4x Retort Stand	**1x** Vernier dual-range force sensor	**1x** Metal cylinder
4x Clamp and Clamp Holder	**1x** Vernier Go-Link	**1x** Lifting jack
1x Protractor	**1x** Laptop	**1x** Chair
1x Stopwatch	**1x** Camera	**1x** Tripod

Procedure and Precautions

1. Prepare the apparatus and set up according to the following figure:
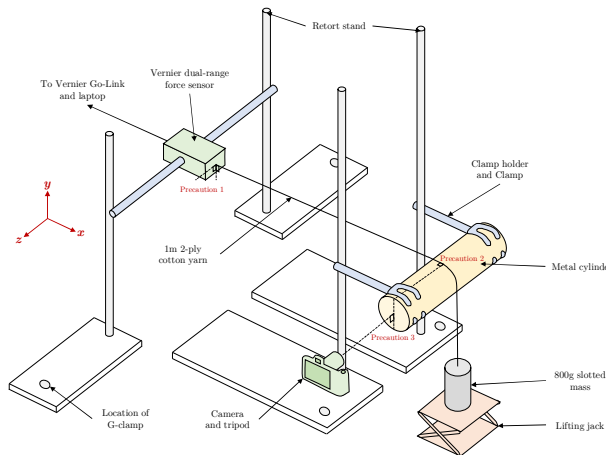
Figure 5. A diagram showing the setup of the experiment for $\theta = \frac{\pi}{2}$.

2. Move the lifting jack to its highest position, such that there is no holding or loading force.
3. On the laptop, *zero* the reading and start collecting data continuously.
4. Move the lifting jack downwards at a very slow rate, increasing the holding force.
5. When the holding force is observed to reach a plateau, maintain its position for 20 seconds.
6. Capture an image that covers a significant portion of the string.
7. Repeat Steps 2-5 for three trials.
8. Repeat Steps 1-6 for all values of the wrap angle.

There are several precautions, and with reference to the positions Figure 5 marked with red:

1. Ensure that the dual-range force sensor is horizontally parallel to the ground (*x-y* direction). and is perpendicular to the string (*x-z* direction).
2. Ensure that the string is perpendicular to the cylinder (*x-z* direction).
3. Ensure that the lens of the camera is pointed at the cylinder's centre, is set to the highest resolution, lowest aperture to blur the background and focused onto the string's thread.

Ethical, safety and environmental concerns

Since the only waste product in this experiment is string, which is biodegradable, there are no significant environmental or ethical concerns. Regarding safety concerns, there is a possibility that the string may break, causing the slotted mass to drop, but the possibilities have already been minimised by thoroughly researching the tensile strength in the pilot study, placing a lifting jack beneath the slotted masses, as well as securely fastening the important components with G-clamps.

Raw Data Table

		Independent Variable – Wrap Angle		
Target	**Coordinates A**	**Coordinates B**	**Average of coordinates A and B**	**Absolute uncertainty in the average of coordinates**
θ_{target} rad	$n(x_{n_A}, y_{n_A})$ px	$n(x_{n_B}, y_{n_B})$ px	$n(x_n, y_n)$ px	$n(\Delta x_n, \Delta y_n)$ ±px
$\frac{\pi}{4}$	1(217, 0), 2(2628, 1628) 3(3079, 2116), 4(3175, 4000)	1(235, 0), (2644, 1631) 3(3090, 2081), 4(3185, 4000)	1(226, 0), 2(2636, 1634.5) 3(3084.5, 2098.5), 4(3180, 4000)	1(9, 0), 2(8, 3.5) 3(5.5, 17.5), 4(5, 0)
$\frac{\pi}{2}$	1(603, 2047), 2(2576, 2006) 3(3352, 2377), 4(3425, 4000)	1(601, 2054), 2(2575, 2020) 3(3360, 2362), 4(3435, 4000)	1(602, 2050.5), 2(2575.5, 2013) 3(3356, 2369.5), 4(3430, 4000)	1(1, 3.5), 2(0.5, 7) 3(4, 7.5), 4(5, 0)
$\frac{3\pi}{4}$	1(589, 3940), 2(2770, 1845) 3(3267, 1981), 4(3311, 4000)	1(596, 3945), 2(2771, 1860) 3(3275, 1957), 4(3317, 4000)	1(592.5, 3942.5), 2(2770.5, 1852.5) 3(3271, 1969), 4(3314, 4000)	1(3.5, 2.5), 2(0.5, 7.5) 3(4, 12), 4(3, 0)
π	1(2634, 4000), 2(2827, 1950) 3(3275, 1990), 4(3269, 4000)	1(2643, 4000), 2(2836, 2000) 3(3285, 1983), 4(3277, 4000)	1(2638.5, 4000), 2(2831.5, 1975) 3(3280, 1986.5), 4(3273, 4000)	1(4.5, 0), 2(4.5, 25) 3(5, 3.5), 4(4, 0)
$\frac{5\pi}{4}$	1(538, 3857), 2(3145, 2075) 3(2827, 1948), 4(2880, 4000)	1(543, 3865), 2(3161, 2075) 3(2838, 1966), 4(2891, 4000)	1(540.5, 3861), 2(3153, 2075) 3(2832.5, 1957), 4(2885.5, 4000)	1(2.5, 4), 2(8, 0) 3(5.5, 9), 4(5.5, 0)
$\frac{3\pi}{2}$	1(717, 2062), 2(3111, 2091) 3(2957, 1896), 4(3010, 4000)	1(714, 2071), 2(3114, 2099) 3(2966, 1908), 4(3017, 4000)	1(540.5, 3861), 2(3153, 2075) 3(2832.5, 1957), 4(2885.5, 4000)	1(1.5, 4.5), 2(1.5, 4) 3(4.5, 6), 4(3.5, 0)
$\frac{7\pi}{4}$	1(515, 0), 2(2889, 2157) 3(2877, 2123), 4(2925, 4000)	1(499, 0), 2(2885, 2140) 3(2863, 2103), 4(2913, 4000)	1(507, 0), 2(2887, 2148.5) 3(2870, 2113), 4(2919, 4000)	1(8, 0), 2(2, 8.5) 3(7, 10), 4(6, 0)

|		Dependent Variable – Holding Force		
Target	**Trial 1**	**Trial 2**	**Trial 3**	**Half Range**
θ_{target} rad	$T_{hold_1} \pm \Delta T_{hold_1}$ N ± N $\Delta_{\text{instrument}} = \pm 0.01$ N	$T_{hold_2} \pm \Delta T_{hold_2}$ N ± N $\Delta_{\text{instrument}} = \pm 0.01$ N	$T_{hold_3} \pm \Delta T_{hold_3}$ N ± N $\Delta_{\text{instrument}} = \pm 0.01$ N	$T_{hold} \pm \Delta T_{hold}$ N ± N $\Delta_{\text{instrument}} = \pm 0.01$ N
$\frac{\pi}{4}$	6.59 ± 0.03	6.59 ± 0.04	6.60 ± 0.04	6.60 ± 0.05
$\frac{\pi}{2}$	6.12 ± 0.02	6.09 ± 0.02	6.07 ± 0.02	6.09 ± 0.04
$\frac{3\pi}{4}$	5.21 ± 0.01	5.35 ± 0.02	5.27 ± 0.02	5.29 ± 0.09
π	4.58 ± 0.03	4.58 ± 0.02	4.59 ± 0.02	4.58 ± 0.03
$\frac{5\pi}{4}$	3.35 ± 0.02	3.57 ± 0.02	3.66 ± 0.02	3.50 ± 0.18
$\frac{3\pi}{2}$	3.49 ± 0.02	3.60 ± 0.02	3.26 ± 0.02	3.43 ± 0.18
$\frac{7\pi}{4}$	2.82 ± 0.02	2.91 ± 0.06	3.00 ± 0.02	2.91 ± 0.11

Qualitative Observation

During the experiment, the holding force is observed to decrease logarithmically as the wrap angle increases. However, several assumptions outlined in the framework appears to be violated. As an example, when the holding force is being increased, the elastic nature of the string caused it to extend by a few millimetres, violating assumption 3. Moreover, between trials where the loading

force is zero (Step 3), it has been observed that the string to some extent stayed at its initial position and did not bend freely, suggesting that it is rigid, violating assumption 2. Most importantly, the rate at which the lifting jack is being operated is different between each trial. This means that if the loading force is being applied in a very short period of time, the slotted mass is allowed to accelerate quickly. Due to this increased downwards acceleration, the tension in the string is higher than normal, violating assumption 3, where the loading force is assumed to be at the verge of the string slipping. This led to an observable fluctuation between trials when $\theta_{target} = \frac{3\pi}{2}$.

Processed Data Table

Wrap Angle	Absolute uncertainty in Wrap Angle	$-\ln$(Holding Force)	Absolute uncertainty in $-\ln$(Holding Force)
θ rad	$\pm\Delta\theta$ $\pm$rad	$-\ln T_{hold}$ $-\ln$ N	$\pm\,\Delta\ln T_{hold}$ $-\ln$ N
0.925	0.005	-1.887	0.006
1.544	0.006	-1.807	0.007
2.314	0.003	-1.67	0.02
3.050	0.003	-1.522	0.007
4.139	0.004	-1.25	0.05
4.749	0.004	-1.23	0.05
5.473	0.005	-1.07	0.04

Below is a sample calculation when $\theta_{target} = \frac{\pi}{4}$:
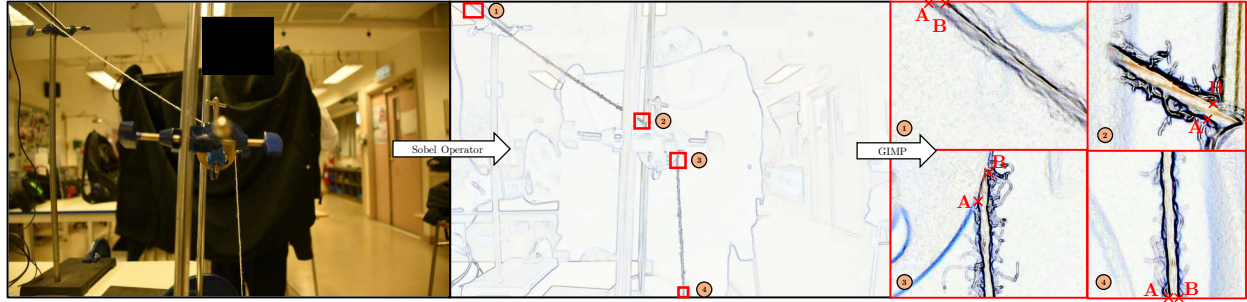
Figure 5. A diagram showing the manual process of extracting 8 coordinates of the edges of the string from an image that is passed through the Sobel Operator.

The coordinates of the centre of the string can be found by taking the half-range of the coordinates of the string edges:

$$\begin{pmatrix} x_1 \pm \Delta x_1, y_1 \pm \Delta y_1 \\ x_2 \pm \Delta x_2, y_2 \pm \Delta y_2 \\ x_3 \pm \Delta x_3, y_3 \pm \Delta y_3 \\ x_4 \pm \Delta x_4, y_4 \pm \Delta y_4 \end{pmatrix} = \begin{pmatrix} \frac{x_{1_A}+x_{1_B}}{2}, \frac{y_{1_A}+y_{1_B}}{2} \\ \frac{x_{2_A}+x_{2_B}}{2}, \frac{y_{2_A}+y_{2_B}}{2} \\ \frac{x_{3_A}+x_{3_B}}{2}, \frac{y_{3_A}+y_{3_B}}{2} \\ \frac{x_{4_A}+x_{4_B}}{2}, \frac{y_{4_A}+y_{4_B}}{2} \end{pmatrix} \pm \begin{pmatrix} |\frac{x_{1_A}-x_{1_B}}{2}|, |\frac{y_{1_A}-y_{1_B}}{2}| \\ |\frac{x_{2_A}-x_{2_B}}{2}|, |\frac{y_{2_A}-y_{2_B}}{2}| \\ |\frac{x_{3_A}-x_{3_B}}{2}|, |\frac{y_{3_A}-y_{3_B}}{2}| \\ |\frac{x_{4_A}-x_{4_B}}{2}|, |\frac{y_{4_A}-y_{4_B}}{2}| \end{pmatrix} = \begin{pmatrix} 226 \pm 9, & 0 \pm 0 \\ 2636 \pm 8, & 1634.5 \pm 3.5 \\ 3084.5 \pm 5.5, & 2098.5 \pm 17.5 \\ 3180 \pm 5, & 4000 \pm 0 \end{pmatrix}$$

The next step is to transform these 4 sets of coordinates into the wrap angle, detailed below:
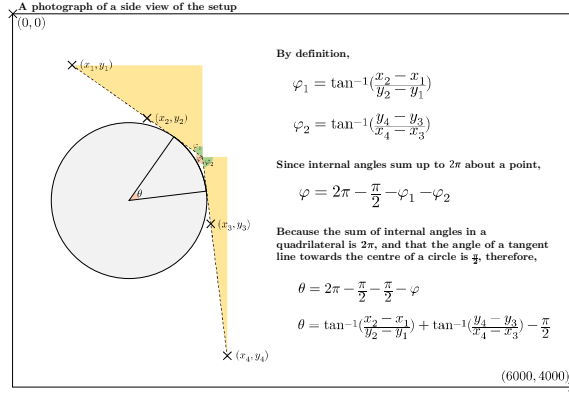
Figure 6. A diagram showing the derivation of the function through a series of trigonometric identities.[3]

Substituting the values, the wrap angle could be determined:

$$\theta = \tan^{-1}\frac{2636 - 226}{1634.5 - 0} + \tan^{-1}\frac{4000 - 2098.5}{3180 - 3084.5} - \frac{\pi}{2} = 0.924659\ldots \approx 0.925 \text{ rad}_{(3s.f.)} \tag{9}$$

Suppose the function $f(x_1, y_1, \ldots)$ outputs the wrap angle given the 4 sets of coordinates, then the propagation of error formula can be used to find the uncertainty in angle, $\Delta\theta$ (Ku):

$$\Delta\theta = \sqrt{\sum_{k=1}^{4}\left(\frac{\partial f}{\partial x_k}\Delta x_k\right)^2 + \left(\frac{\partial f}{\partial y_k}\Delta y_k\right)^2} \tag{10}$$

Simplified versions of Equation 10 for different values of θ could be found in the Appendix. Substituting in the values:

$$\Delta\theta = \sqrt{\frac{(1634.5 - 0)^2(8^2 + 9^2) + (2636 - 226)^2(0^2 + 3.5^2)}{((2636 - 226)^2 + (1634.5 - 0)^2)^2} + \frac{(3180 - 3084.5)^2(0^2 + 17.5^2) + (4000 - 2098.5)^2(5^2 + 5.5^2)}{((4000 - 2098.5)^2 + (3180 - 3084.5)^2)^2}}$$
$$\Delta\theta = 0.00456995\ldots \approx 0.005 \text{ rad}_{(1d.p.)} \tag{11}$$

The calculation of the holding force starts with the extraction of the holding forces in each trial:
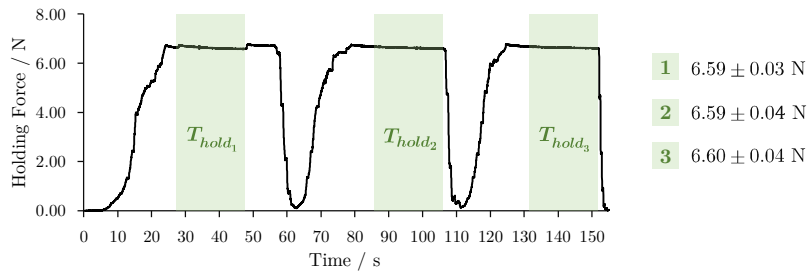
Figure 7. A diagram showing the process of data extraction.

The final holding force and its uncertainty is then calculated:

$$T_{hold_{max}} = \max\left(T_{hold_1} + \Delta T_{hold_1}, T_{hold_2} + \Delta T_{hold_2}, T_{hold_3} + \Delta T_{hold_3}\right) + 0.01 = 6.65\text{N}$$
$$T_{hold_{max}} = \min\left(T_{hold_1} - \Delta T_{hold_1}, T_{hol\ 2} - \Delta T_{hold_2}, T_{hol\ 3} - \Delta T_{hold_3}\right) - 0.01 = 6.55\text{N}$$
$$T_{hold} = \frac{T_{hold_{max}} + T_{hol\ min}}{2} \pm \frac{T_{hold_{max}} - T_{hold_{min}}}{2} = (6.60 \pm 0.05)\text{ N} \tag{12}$$

---

[3] Note that the function that maps the 4 sets of coordinates to angles are case-specific and may vary for different trials. For a detailed list of function definitions, please refer to the Appendix.

In order to better represent the data on a graph and to ease calculations, the relationship must be linearised. It can be achieved by taking the natural logarithm on both sides of the Capstan Equation:

$$T_{hold} = T_{load}e^{-\mu_s\theta}$$
$$\ln T_{hold} = \ln T_{load} + \ln e^{-\mu_s\theta}$$
$$\ln T_{hold} = -\mu_s\theta + \ln T_{load}$$
$$-\ln T_{hold} = \mu_s\theta - \ln T_{load} \tag{13}$$

From the new relationship above, suppose the function $g(T_{hold}) = -\ln T_{hold}$, then the new holding force is $-\ln 6.60 \approx -1.887$ N. The uncertainty could be determined by using the propagation of error formula:

$$\Delta \ln T_{hold} = \sqrt{\left(\frac{\partial g}{\partial T_{hold}}\Delta T_{hold}\right)^2} = \sqrt{\left(-\frac{1}{T_{hold}}\Delta T_{hold}\right)^2}$$
$$\Delta \ln T_{hold} = \frac{\Delta T_{hold}}{T_{hol}} = \frac{0.05}{6.60} = 0.00757575\ldots \approx 0.008 \text{ N} \tag{14}$$
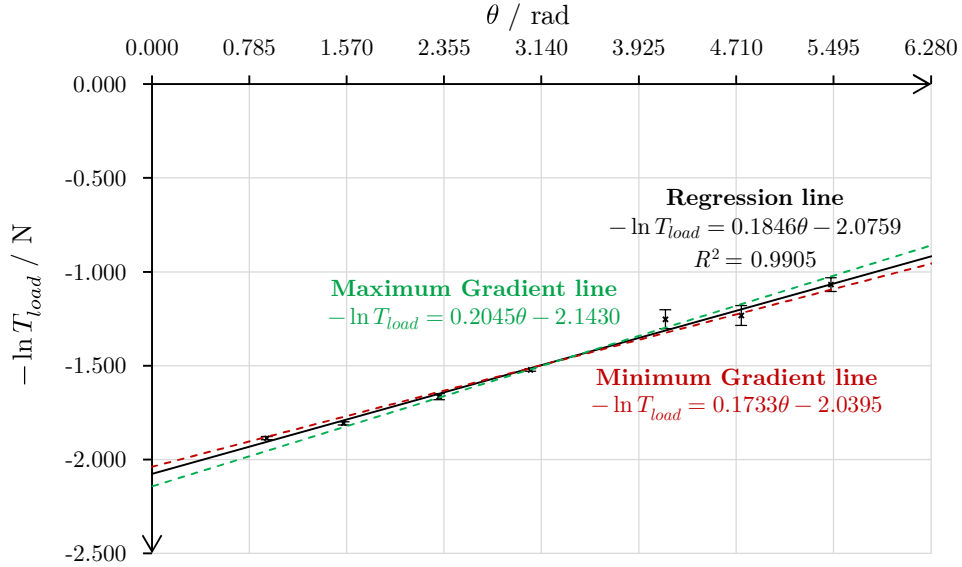
Graph

Figure 8. A linearised plot of the loading force ($-\ln T_{load}$) against wrap angle (θ).

Note: The greatest uncertainty in wrap angle is only ±0.006 radians and considering the horizontal range of the graph (6.283 radians), it only takes up 0.095% of the space. Because this magnitude is too small to be observed, the horizontal error bars are not included.

It has been observed that there is an anomaly at $\theta = 4.139$ rad, where the loading force appears to be lower than usual. If the string is not parallel to the force sensor, it may neglect the horizontal or vertical force component (Precaution 1). There may also be a possibility that the string had touched teach other, causing yarn-to-yarn friction, reducing the loading force. Regarding the choice of line of best fit, although the gradient appears to approach zero on both sides, suggesting a suit for a cubic polynomial fit, the small magnitude of the error bars means that the only suitable line of best fit that fits appropriately within the error bars is linear.

Conclusion

The mathematical relationship between the holding force and the wrap angle can be best described as negative logarithmic. When Equation 13 is being compared to the slope-intercept form ($y = mx + c$, where m is the slope and c is the y-intercept), then the slope of the graph denotes the coefficient of friction (μ_s), while the y-intercept denotes $-\ln T_{load}$.

From the graph, the minimum gradient is 0.1733, while the maximum gradient is 0.2045, therefore the coefficient of friction is 0.19 ± 0.01. Similarly, the y-intercept ranges between:

$$-2.1430 < -\ln T_{load} < -2.0395$$
$$e^{2.0395} < T_{load} < e^{2.1430}$$
$$7.69 < T_{load} < 8.52 \tag{15}$$

therefore, the loading force is (8.1 ± 0.4) N. A test that determines the true value of the loading force has been performed. The slotted mass is suspended vertically by the force sensor, measuring the change in loading force over a 10 second interval. By applying half-range estimation, the true loading force was determined to be (7.88 ± 0.03) N, meaning the loading force previously determined was overestimated by 0.23N. By vertically translating the graph upwards by the natural logarithm of the true loading force, which is (2.064 ± 0.004) N, the range of y-intercepts formed by the maximum and minimum gradient lines would cover the origin, therefore the linearised relationship would be directly proportional if $T_{load} = 0$, meaning an insignificant systematic error.

Comparison with the literature

In the Capstan Equation ($T_{hold} = T_{load}e^{-\mu_s\theta}$), the static coefficient of friction (μ_s) is the only constant, therefore in order to check if the results are reasonable, the literature values of it have been extensively researched. A full list of the values and conditions can be found in the Appendix.
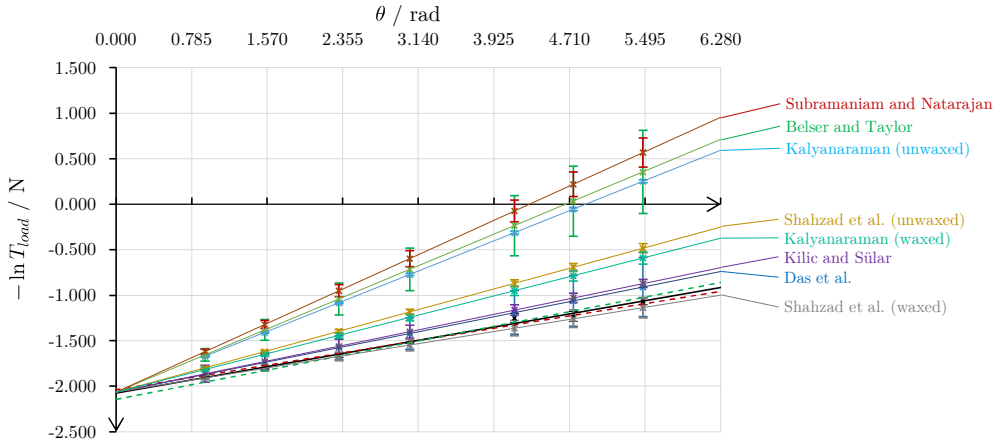
Figure 9. A linearised plot of the loading force ($-\ln T_{load}$) against wrap angle (θ), including the predicted loading force from various researchers, based on their literature values and respective uncertainties.

Qualitatively, the experimental slope matches the general trend of the researchers, where the coefficient of friction is positive. Because it has been observed that the coefficient of friction varies largely between the researchers, a large amount of literature values of μ_s have been collected. In fact, since the static coefficient of friction is based on the type of two contacting materials, slight

differences in the physical properties of either the string or the capstan can cause the value to change by a huge magnitude. In other words, there is not a universal constant coefficient of friction that governs all material types. Therefore, although only two (Das et al., Shahzad et al.) literature values lie within the region enclosed by the maximum and minimum gradient line, it is safe to assume that the experimental data is reasonable.

However, it is still noticeable that a majority of the researcher's value of coefficient of friction (7 of 8) are above the experimental value. There are a number of factors that can cause this, including environmental aspects and string properties. On the microscopic level, as the relative humidity is increased, water molecules adhere to the cellulose fibres of the cotton yarns, increasing ruggedness and hence increasing the coefficient of friction (Kenins; Besler & Taylor). In fact, a majority of the researcher's experiments are conducted under the internationally agreed ASTM D1776 standard, at 65% relative humidity. However, the relative humidity during the experiment was only 42%, explaining why the coefficient of friction might have been lower than the literature. Additionally, the string used in the experiment is composed of two smaller threads, each twisted towards each other to give better tensile strength. When the number of twists per unit length is increased, threads are closely interlocked, making it hard for frictional forces to move the individual threads, hence a higher coefficient of friction (Subramaniam). In fact, Subramaniam used yarn of 8.75 to 12.5 twists cm^{-1}, but by analysing the yarn used in the experiment, it ranged from roughly 1 to 2 twists cm^{-1}, explaining why the coefficient of friction might be lower than the researcher's values.

Sources of error and Limitations

Source of error	Significance	Improvements
The holding force is not the minimum force needed to cause the system to not slip.	Very significant in affecting the random error. When the lifting jack is suddenly removed, or no longer in contact with the slotted mass, it begins to accelerate downwards. Because of kinetic friction, the kinetic energy of the slotted mass decreases and comes to a halt. However, because the rebounding spring force is less than the maximum static friction, the string does not move and is held at an extended position, causing the tension to be higher than normal.	There are two ways to minimise this problem, to reduce the rate of change in tension over time by placing a sponge between the lifting jack and the mass. Another approach to this methodological issue is to attach a motor to the capstan. The motor will then start to spin at a very slow speed in the direction of the holding force. As this happens, the frictional force begins to rise, causing the holding force to decrease. As this frictional force rises past the maximum static friction, dynamic friction occurs, causing the slotted mass to drop back to its initial position. This causes a sharp increase in the holding force, and therefore the absolute minimum loading force could then be determined.
Measured loading force is sometimes below the true loading force.	As a continuation of the above, during some of the trials when the slotted mass is being lowered, the lifting jack can get stuck at a specific position, causing "stuttering" on the holding	Using a motorised lifting jack will ensure the tension is gradually applied. However, the best option will be to use the suggested new experimental method above, which

	force, and because of the effect described above, the final holding force will increase.	essentially eliminates the need to account for it.
The loading force appears to decrease as time passes during each individual trial.	Significant in affecting the random error. Because the string is elastic, it has the tendency to return to its equilibrium position. Microscopically, as threads lose contact with the capstan, the frictional force is decreased, hence the rebounding force is increased.	Since the force appears to reach a stable value, extending the data collection time to 1 minute and taking the last 10 seconds will reduce the uncertainty. To minimise the rebounding force, another string should be chosen with a higher stiffness, for example, braided strings.
The loading force appears to always increase between trials.	Significant in affecting the random error. In almost every trial, consecutive trials show that the loading force increases.	Replace the string for each trial to ensure that the quality of the string is consistent. Also ensure that the slotted mass retains its rotational position, so that the twist factor is kept constant.
Improper Angles in capstan and force sensor	Significant in affecting the random error. If the string is tilted, it may neglect some force components, leading to wrong measurements.	Use a protractor to properly angle and position the instruments. Capture a birds-eye view of the setup to ensure that the ensure the angles are appropriate as well.
The coefficient of friction of the string is not uniform on the capstan.	Insignificant in affecting the random error. Because of the nature of two-ply strings, some parts of the string may experience a larger normal force.	Use strings with a higher twist factor, meaning threads will be closer to each other and hence better evenly distribute the normal force.

Improvement and Extension

Despite major changes in experimental design and proposals of multiple improvements above, that are aimed at reducing as many possible sources of errors as possible, there are still some violations to the assumptions of the Capstan Equation that are currently that are hard to avoid and in partially out of the scope of the current study. As an example, according to Gupta et al., conventional cotton yarns and woven fabrics are known to not obey the Amonton's Classical Law of Friction (Equation 6), hence rendering the traditional Capstan Equation inaccurate. Instead, the group has arrived at a modified relationship:

$$T_{hold} = T_{load}e^{\theta a(\frac{r}{T_{load}})^{1-n}} \tag{16}$$

Where r is the capstan radius, n is some constant (n for textile materials range between 0.8 and 0.96), and a is some constant that approaches μ_s when n approaches 1.

According to the experimental results of Gupta et al., this equation causes an average of 10% discrepancy between the actual result. Because of this, small errors in the independent variable can cause the dependent variable to not obey the proposed relationship. In order to accurately study this relationship, the number of trials should be increased and the range of independent variable, θ, should be extended beyond 2π to increase the fidelity of the data.

References

Belser, R B, and J L Taylor. R. B. Belser, 1968, pp. 1–198, *FRICTIONAL PROPERTIES OF COTTON FIBERS*.

Das, Apurba, et al. "A STUDY ON FRICTIONAL CHARACTERISTICS OF WOVEN FABRICS ." *AUTEX Research Journal*, vol. 5, no. 3, Sept. 2005, pp. 1–8., www.autexrj.com/cms/zalaczone_pliki/3-05-3.pdf.

Gao, Xiaoping, et al. "An Improved Capstan Equation Including Power-Law Friction and Bending Rigidity for High Performance Yarn." *Mechanism and Machine Theory*, vol. 90, Elsevier BV, Aug. 2015, pp. 84–94., doi:10.1016/j.mechmachtheory.2015.03.005.

GUPTA, BS, et al. "Experimental Methods for Analyzing Friction in Textiles." Friction in Textile Materials, Elsevier, 2008, 174–221. Crossref, doi:10.1533/9781845694722.1.174.

Huang, Wei, et al. "An Approach to Predict the Tensile Strength of a Two-Ply Yarn from Single Filament Yarn." *The Journal of The Textile Institute*, vol. 108, no. 3, Informa UK Limited, Mar. 2016, pp. 412–417., doi:10.1080/00405000.2016.1169010.

Jung, Jae Ho, et al. "Capstan Equation Including Bending Rigidity and Non-Linear Frictional Behavior." *Mechanism and Machine Theory*, vol. 43, no. 6, Elsevier BV, June 2008, pp. 661–675., doi:10.1016/j.mechmachtheory.2007.06.002.

Jung, Jae Ho, et al. "Effect of Bending Rigidity on the Capstan Equation." *Textile Research Journal*, vol. 74, no. 12, SAGE Publications, Dec. 2004, pp. 1085–1096., doi:10.1177/004051750407401210.

Jung, Jae Ho, et al. "Generalized Capstan Problem: Bending Rigidity, Nonlinear Friction, and Extensibility Effect." *Tribology International*, vol. 41, no. 6, Elsevier BV, June 2008, pp. 524–534., doi:10.1016/j.triboint.2007.11.005.

Kalyanraman, A R. "Coefficient of Friction between Yarns and Contact Surfaces." *Indian Journal of Textile Research*, vol. 13, Mar. 1988, pp. 1–6.

Kenins, P. "Influence of Fiber Type and Moisture on Measured Fabric-to-Skin Friction." *Textile Research Journal*, vol. 64, no. 12, SAGE Publications, Dec. 1994, pp. 722–728., doi:10.1177/004051759406401204.

Kilic, Gonca Balci, and Vildan Sülar. "Frictional Properties of Cotton-Tencel Yarns Spun in Different Spinning Systems." *Textile Research Journal*, vol. 82, no. 8, SAGE Publications, Jan. 2012, pp. 755–765., doi:10.1177/0040517511429610.

Ku, H. H. "Notes on the Use of Propagation of Error Formulas." *Journal of Research of the National Bureau of Standards*, Section C: Engineering and Instrumentation, vol. 70C, no. 4, National Institute of Standards and Technology (NIST), Oct. 1966, p. 263., doi:10.6028/jres.070c.025.

1. Liu, Junpeng, and Murilo Augusto Vaz. "Three-Dimensional Determination of Superposed Helical Wires Constraint Ability." Latin American Journal of Solids and Structures, vol. 15, no. 3, FapUNIFESP (SciELO), May 2018. Crossref, doi:10.1590/1679-78254085.

Ramkumar, S. S., et al. "Experimental Verification of Failure of Amontons' Law in Polymeric Textiles." *Journal of Applied Polymer Science*, vol. 91, no. 6, Wiley, 2004, pp. 3879–3885., doi:10.1002/app.13566.

Shahzad, Amir, et al. "Statistical Analysis of Yarn to Metal Frictional Coefficient of Cotton Spun Yarn Using Taguchi Design of Experiment." *The Journal of Strain Analysis for Engineering Design*, vol. 53, no. 7, SAGE Publications, July 2018, pp. 485–493., doi:10.1177/0309324718786373.

Subramaniam, V., and K. S. Natarajan. "Frictional Properties of Siro Spun Yarns." *Textile Research Journal*, vol. 60, no. 4, SAGE Publications, Apr. 1990, pp. 234–239., doi:10.1177/004051759006000407

Sun, Yi, et al. "Theoretical and Experimental Investigations on the Effects of Friction, Bending Rigidity, Extensibility, and Poisson's Ratio on Fabric Tensile Properties." *Textile Research Journal*, SAGE Publications, Aug. 2020, p. 004051752094945., doi:10.1177/0040517520949450.

"Dual-Range Force Sensor." *Vernier*, www.vernier.com/product/dual-range-force-sensor/.

"Practice for Conditioning and Testing Textiles". *ASTM International*., doi:10.1520/d1776-08.

"Po Leung Kuk Choi Kai Yau School, Piper's Hill." Ambient Weather, 4 Feb. 2021, ambientweather.net/dashboard/06f4cfb56e903bb394f6fd710266e8db/graphs.

Appendix

Target	Function of angle	Function of uncertainty in angle
$\dfrac{\pi}{4}$	$\tan^{-1}\dfrac{x_2-x_1}{y_2-y_1}+\tan^{-1}\dfrac{y_4-y_3}{x_4-x_3}-\dfrac{\pi}{2}$	$\sqrt{\dfrac{(y_2-y_1)^2(\Delta x_2{}^2+\Delta x_1{}^2)+(x_2-x_1)^2(\Delta y_2{}^2+\Delta y_1{}^2)}{((x_2-x_1)^2+(y_2-y_1)^2)^2}+\dfrac{(x_4-x_3)^2(\Delta y_4{}^2+\Delta y_3{}^2)+(y_4-y_3)^2(\Delta x_4{}^2+\Delta x_3{}^2)}{((y_4-y_3)^2+(x_4-x_3)^2)^2}}$
$\dfrac{\pi}{2}$	$\tan^{-1}\dfrac{y_1-y_2}{x_2-x_1}+\tan^{-1}\dfrac{y_4-y_3}{x_4-x_3}$	$\sqrt{\dfrac{(x_2-x_1)^2(\Delta y_1{}^2+\Delta y_2{}^2)+(y_1-y_2)^2(\Delta x_2{}^2+\Delta x_1{}^2)}{((y_1-y_2)^2+(x_2-x_1)^2)^2}+\dfrac{(x_4-x_3)^2(\Delta y_4{}^2+\Delta y_3{}^2)+(y_4-y_3)^2(\Delta x_4{}^2+\Delta x_3{}^2)}{((y_4-y_3)^2+(x_4-x_3)^2)^2}}$
$\dfrac{3\pi}{4}$	same as $\frac{\pi}{2}$	same as $\frac{\pi}{2}$
π	$\tan^{-1}\dfrac{y_1-y_2}{x_2-x_1}+\tan^{-1}\dfrac{x_3-x_4}{y_4-y_3}+\dfrac{\pi}{4}$	$\sqrt{\dfrac{(x_2-x_1)^2(\Delta y_1{}^2+\Delta y_2{}^2)+(y_1-y_2)^2(\Delta x_2{}^2+\Delta x_1{}^2)}{((y_1-y_2)^2+(x_2-x_1)^2)^2}+\dfrac{(y_4-y_3)^2(\Delta x_3{}^2+\Delta x_4{}^2)+(x_3-x_4)^2(\Delta y_4{}^2+\Delta y_3{}^2)}{((x_3-x_4)^2+(y_4-y_3)^2)^2}}$
$\dfrac{5\pi}{4}$	$2\pi-\tan^{-1}\dfrac{y_1-y_2}{x_2-x_1}-\tan^{-1}\dfrac{y_4-y_3}{x_4-x_3}$	same as $\frac{\pi}{2}$
$\dfrac{3\pi}{2}$	$\tan^{-1}\dfrac{y_2-y_1}{x_2-x_1}+\tan^{-1}\dfrac{x_4-x_3}{y_4-y_3}+\dfrac{3\pi}{2}$	$\sqrt{\dfrac{(x_2-x_1)^2(\Delta y_2{}^2+\Delta y_1{}^2)+(y_2-y_1)^2(\Delta x_2{}^2+\Delta x_1{}^2)}{((y_2-y_1)^2+(x_2-x_1)^2)^2}+\dfrac{(y_4-y_3)^2(\Delta x_4{}^2+\Delta x_3{}^2)+(x_4-x_3)^2(\Delta y_4{}^2+\Delta y_3{}^2)}{((x_4-x_3)^2+(y_4-y_3)^2)^2}}$
$\dfrac{7\pi}{4}$	same as $\frac{3\pi}{2}$	same as $\frac{3\pi}{2}$

Table 1: A list of functions that processes the four sets of coordinates to angles and its relevant uncertainty.

Researcher(s)	Literature value of the static coefficient of friction	Assumptions/Test Conditions
Shahzad et al.	0.170 ± 0.019	Waxed finish $(65 \pm 2)\%\ RH, (20 \pm 2)°C$
Das et al.	0.211 ± 0.051	$T_{load} = 0.6\ N$
Kilic and Sülar	0.218 ± 0.009	$T_{load} = 9\ N$, twist factor=4.0
Kalyanaraman	0.269 ± 0.011	Waxed finish $60\%\ RH, 35°C, T_{load} = 0.045\ N$
Shahzad et al.	0.2886 ± 0.0082	Unwaxed finish $(65 \pm 2)\%\ RH, (20 \pm 2)°C$
Kalyanaraman	0.423 ± 0.024	Unwaxed finish $60\%\ RH, 35°C, T_{load} = 0.045\ N$
Belser and Taylor	0.442 ± 0.068	$(60 \pm 5)\%\ RH, (25 \pm 2)°C, T_{load} = 0.000425\ N$
Subramaniam and Natarajan	0.481 ± 0.026	$T_{load} = 0.04\ N$, twist factor=45

Table 2: A list of the literature values of static coefficient of friction obtained from various researchers and their respective test conditions.